The Influence of Widow Size on Remote Sensing-Based Prediction of Forest Structural Variables

Ulaş Yunus ÖZKAN (uozkan@istanbul.edu.tr)
Istanbul University-Cerrahpaşa https://orcid.org/0000-0002-8709-0285
Tufan Demirel
Istanbul University-Cerrahpaşa, Faculty of Forestry

Research

Keywords: Optimal window size, Random forest, WorldView-3, Digital aerial image, LiDAR

Posted Date: February 25th, 2021

DOI: https://doi.org/10.21203/rs.3.rs-236373/v1

Version of Record: A version of this preprint was published at Ecological Processes on September 8th, 2021. See the published version at https://doi.org/10.1186/s13717-021-00330-4.

Abstract

Background: Determining the appropriate window size is a critical step for estimating stand structural variables based on remote sensing data. Because the value of the reference laser and image metrics that affect the quality of the prediction model depends on window size. However, suitable window sizes are usually determined by trial and error. There are a limited number of published studies evaluating appropriate window sizes for different remote sensing data. This research investigated the effect of window size on predicting forest structural variables using airborne LiDAR data, digital aerial image and WorldView-3 satellite image.

Results: In the WorldView-3 and digital aerial image, significant differences were observed in the prediction accuracies of the structural variables according to different window sizes. For the estimation based on WorldView-3 in black pine stands, the optimal window sizes for stem number (N), volume (V), basal area (BA) and mean height (H) were determined as 1000 m^2, 100 m^2, 100 m^2 and 600 m^2, respectively. In oak stands, the R^2 values of each moving window size were almost identical for N and BA. The optimal window size was 400 m^2 for V and 600 m^2 for H. For the estimation based on aerial image in black pine stands, the 800 m^2 window size is optimal for N and H, the 600 m^2 window size is optimal for V and the 1000 m^2 window size is optimal for BA. In the oak stands, the optimal window sizes for N, V, BA and H were determined as 1000 m^2, 100 m^2, 100 m^2 and 600 m^2, respectively. The optimal window sizes may need to be scaled up or down to match the stand canopy components. In the LiDAR data, the R^2 values of each window size were almost identical for all variables of the black pine and the oak stands.

Conclusion: This study illustrated that the window size has an effect on the prediction accuracy in estimating forest structural variables based on remote sensing data. Moreover, the results showed that the optimal window size for forest structural variables varies according to remote sensing data and tree species composition.

Background

Forests are important ecosystems thanks to their many services such as soil conservation, improving air and water quality, decreasing noise pollution, carbon storage (Lee et al. 2010). For sustainable management of these ecosystems, data on horizontal and vertical forest structure are required. (Pascual et al. 2008; Koch et al. 2009). Because the forest structure has an important effect on ecosystem services (García et al. 2018). Forest structural data are traditionally provided from field data of limited spatial extent. However, the traditional methods involving forest inventories that require labor-intensive field surveys are quite time consuming and expensive (Kwak et al. 2007; Joshi et al. 2015; García et al. 2018). Remote sensing data has been used as an auxiliary data source in forest inventory since early days of remote sensing (Kayitakire et al. 2006; Su et al. 2020). Stand structural variables such as crown canopy, species composition, stem density and basal area can be estimated on the forest stand level using remote sensing data. Therefore, the remote sensing data have great potential to reduce inventory cost and improve estimation accuracy (Steinmann et al. 2013; Saarela et al. 2020).

Aerial photograph is oldest remote sensing data used in forest inventory and has still an important role in forest planning (Morgan et al. 2010; Ozkan and Demirel 2018). Current digital aerial cameras can provide digital images of very high spatial resolution (Balenović et al. 2015). Satellite images with very high spatial resolution are a cost-effective alternative source to aerial photographs. Satellite images have important advantages such

as broad spatial coverage and temporally high frequency (Junttila et al. 2013; García et al. 2018). Light Detection and Ranging (LiDAR) data can better capture the three-dimensional (3-D) structure of forest canopies than passive optical sensors, given their ability to penetrate the canopy to different depths (Zald et al. 2014; García et al. 2018). So, LiDAR which among of the available remote sensing data, is a powerful data source for measuring and predicting forest structural features (Joshi et al. 2015).

Due to these advantages, numerous studies have been conducted to evaluate the potential of each remote sensing data in the forest inventory. The studies were first carried out based on visual interpretation. In stand volume estimates based on the visual interpretation of the aerial photograph, the relative error has been reported as between 14% and 45% and in the prediction based on the satellite image interpretation, the corresponding error has been reported as between 20% and 70% (Hyyppa et. 2001). The evolving expectations on the time, accuracy and cost effectiveness of forest inventory studies have led visual interpretation to be replaced by semi-automatic and automatic techniques over time (Hájek 2008). However, there is still no agreement in terms of the estimation accuracy that remote sensing data are the best tools to estimate forest structural features (Fassnacht et al. 2014).

The prediction accuracy of structural variables varies considerably depending on the spatial resolution of image, sampling window size, laser and image metrics (Iovan et al. 2008; Zenner et al. 2009; Castillo-Santiago et al. 2010; Steinmann et al. 2013; Meng et al. 2016). Several studies have shown that the sample plot size is important factors for the accuracy of forest inventory (Hájek 2008; García et al. 2018; Robinson et al. 2013). Ruiz et al. 2014 pointed out that the larger sample plot sizes do not significantly increase the estimation accuracy and it should have a minimum size of 500-600 m^2 for volume estimation. Likewise, sampling window size affects the estimation accuracy of models. Because the value of the reference laser and image metrics that affect the prediction model quality depends on sampling window size (Castillo-Santiago et al. 2010; Steinmann et al. 2013; Meng et al. 2016). While a small window size increases the noise content in the image, too large window size cannot effectively extract the information. Also, a larger window size means more processing time. (Amini and Sumantyo 2009; Meng et al. 2016). Therefore, it is a critical step to determine the optimal window size that matches the forest canopy components, depending on the image spatial resolution.

Several studies have shown the impact of window size on the estimation accuracy of forest structural variables using remote sensing data. Holopainen and Wang (1998) stated that the optimal window size depends on forest stand class, spectral band and image scale, and window size of 20x20 m is the near-optimal window size for feature extraction from aerial photograph in forest inventory. Kayitakire et al. (2006) investigated the estimation of forest structural variables by means of texture features from IKONOS-2. It was stated that stand age is best explained by window size of 15x15 pixels, density by window size of 5x5 pixels, height by window size of 15x15 pixels and basal area by window size of 25 x25. Rich et al. (2010) determined that the pat-terns in image texture of IKONOS satellite image did not change from 25 to 225 m^2 window size. In the study conducted by Tonolli et al. (2011) the accuracy of the estimation of tree stem volume was assessed using LiDAR data. The study results revealed that optimal cell size is 40x40 m. Steinmann et al. (2013) stated that the window size of 25X25 m is optimal for estimating the forest growing stock volume using LiDAR data and aerial images. Meng et al. (2016) tested seven window sizes (from 3x3 to 15x15 pixels) to estimate forest structure from the SPOT-5 satellite image. In order to determine the optimum window size, they calculated the Pearson correlation coefficient of texture statistics with biomass and stated that 9x9 pixel window size is the minimum window size

that provides the highest correlation coefficient. Zhao et al. (2018) identified the optimal window size for estimating canopy cover using QuickBird multispectral and panchromatic images. Window size of 15x15 pixels for panchromatic image and window size of 9x9 pixels for multispectral image were chosen as the optimal window size. According to these studies, optimal window size depends on remote sensing data and forest structural variables to be estimated. However, this issue has not been evaluated sufficiently yet. Further studies are needed to determine the optimal window sizes for estimation of forest structure features using remote sensing data.

The objective of this research is to investigate the effects of window size on estimation accuracy of forest structural variables based on LiDAR data, digital aerial image and WorldView-3 satellite image. More specifically, i) sampling windows of different sizes (200, 400, 600, 800 and 1000 m^2) were developed from remote sensing data; ii) estimation models were developed based on reference laser and image metrics extracted from image windows were developed; iii) the effect of window size on accuracy of the models was analyzed and the optimal window sizes were determined for estimating forest structural variables.

Materials And Methods

Study Area

The study area is located on the Thrace side of the Marmara region of Turkey (41° 09' 15"– 41° 11' 01" N and 28° 59' 17" – 29° 32' 25" E) (Fig. 1). It has an elevation ranging from 10 to 237 m above sea level. In the study area with a total area of 2172 hectares, the forest area cover constitutes 88% of the total area. Red pine, Black pine, Stone Pine, Maritime Pine, Oak, Chestnut, Beech, Linden, and Hornbeam species constitute a large number of stands in pure or mixed form. Most of the forest area consists of broadleaf stands which are dominated by oak species. Among the coniferous species, Black pine and Maritime pine are the dominant species. Also stand management regime of the forest is even-aged. Detailed information for the research area was presented by Ozkan et al. (2020)

Field Reference Data

A field survey was performed between June and August 2018 on the sample plots. A total of 45 samples were randomly selected from pure black pine and oak stands within a study area of 2172 hectares using stand maps produced based on the combination of aerial photograph and forest inventory data in the forest management plan. These stands were visited by a field crew and sample plots were established and the central points were located using GNSS / CORS GPS in each stand. The accuracy of the positioning was approximately 0.25 m.The sample plots were consisted of six concentric circles with an area of 200 m^2 to 1000 m^2. All trees with a diameter at breast height (DBH) ≥ 8 cm were recorded within each of the sample plots of different sizes and their heights measured with a Haglöf Vertex VL5 Laser field measuring instrument. For the sample plot, stem number (N), basal area (BA, m^2), volume (V, m^3) and mean height (H, m) parameters were determined. Basal area was calculated from the diameter measurements of all trees. These values that calculated for each tree in the sample plot were summed. Volume of each tree was computed based on species-specific equations obtained from the forest management plan. Total plot volume was calculated as the sum of the individual tree volumes. The mean height was determined as the arithmetic mean height of all measured trees in the sample plot. The descriptive statistics of the ground truth data are depicted in Table 1.

Remote Sensing Data and Processing

The remote sensing data set included airborne and satellite data: digital aerial imagery, LiDAR and WorldView-3. High point density airborne LiDAR data for the study area were acquired on 22 July 2018, using the LMS-Q680i laser scanner system at a nominal altitude of 720 m above ground level. The system operated at 400 kHz laser pulse repetition rate and a wavelength of 1550 nm. While the point density varied throughout the study area, the minimum point density was 12 points/m^2. Multiple turns were recorded as well as intensity values for each pulse. The maximum scan angles were ± 20^o off-nadir. All artificial objects such as buildings, power lines, base stations have been removed from the raw LiDAR point cloud data using Global Mapper software. After this process, the LiDAR point cloud was divided into two classes, ground and vegetation, to obtain a Normalized point cloud (NPC). While the last return points were classified as ground points, points other than ground class were assigned to the vegetation class using the NDVI (Normalized Difference Vegetation Index) image. The digital terrain model (DTM), as a representation of the ground area, was generated with the TIN (triangulated irregular networks) from the ground class points (Kwak et al. 2007). After obtaining the DTM, the relative height of each point was determined as the difference between the point's height and the terrain surface height. So the NPC representing the height above ground level was obtained. Finally, in order to eliminate the effects of objects such as shrubs and rocks, the vegetation height threshold (average 2 m) was applied to the NPC value, which represents the tree canopy height in forest areas (Næsset 2002).

Aerial images were acquired on May 2015 using UltraCam X (Microsoft, Vexcel Imaging GmbH) digital aerial camera. The camera has 7.2 µm physical sensor pixel size. Aerial images are totally comprised of four bands which are Red (580-700 nm), Green (480-630 nm), Blue (410-540 nm) and Infrared (690-1000 nm) bands. These images were taken as stereo from altitude of 4200 meters above ground level with 70 % forward and 30 % side overlap. For each raw stereo image pairs, geometric calibration and radiometric correction utilized in ERDAS LPS (Hexagon Geospatial) software using interior (focal length, coordinates of the principal point) and exterior (position and rotation of the camera) orientation parameters.

WorldView-3 multispectral image was acquired over the study area on June 2018 with 1.24 m spatial resolution. The multispectral image had four bands, including blue (0.45–0.51 µm), green (0.51–0.58 µm), red (0.63–0.69 µm) and near-infrared (0.78–0.92 µm) bands. Atmospheric correction was carried out using the physical model based approach as implemented in ATCOR (PCI Geomatics 2017). Solar Zenith and Azimuth values of the satellite image, radiometric calibration values for each spectrum gathered from WorldView-3's metadata and DTM generated from the LiDAR data were used to create a fog and aerosol-free satellite image, and object reflectance values were obtained using PCI Geomatica software. After this atmospheric correction proces, the orthorectification was performed using DTM and ground control points. In order to provide more detailed data on vegetation-covered areas, NDVI, the most commonly used vegetation index, was produced using NearIR-1 and Red bands of WorldView-3 (Cho et al. 2009).

Predictor Variables

The laser and image metrics corresponding to the sample plots were extracted from three different remote sensing data. These metrics that used as predictor variables were obtained from circular image windows with different moving window sizes centered on each sample plot. For this, first of all, the sample plots which have high accuracy center coordinates, were spatially registered on remote sensing data by means of GIS. Thus,

concentric window sets were created which consisted of six image windows with a size of 100 m^2 to 1000 m^2 (equal to the size of the graund sample plot) (Fig. 2). LiDAR metrics, that be used as potential variables in predictive models of forest structural variables, were computed for each LiDAR window. LiDAR metrics were derived from the normalized point clouds of the LiDAR windows using trial version of the LiDAR360 software. In this study, a total of 102 LiDAR metrics (LiDAR360 2018) were extracted from LiDAR pulses by using two basic properties of LIDAR data: "Height Metrics" and "Density Metrics".

Spectral and textural metrics were extracted from aerial images and WorldView-3 satellite image by averaging their values within image windows. For each image window, the following spectral features were calculated to explain potential variation in the forest structural variables: mean, standard deviation, skewness and NDVI values. The texture properties were determined according to the Gray Level Co-occurrence Matrix (GLCM) (Haralick et al. 1973). GLCM is widely utilized to describe the textural properties in remote sensing studies (Kayitakire et al. 2006; Maltamo et al., 2006; Shamsoddini et al., 2013; Ozdemir and Donoghue 2013; Ozkan et al. 2016; Meng 2016; Zhao et al. 2018; Ozkan et al. 2020). There are many texture properties defined by GLCM in three main groups as Contrast, Orderliness and Descriptive (Ozdemir and Karnieli 2011). These properties can be affected by the spatial resolution and spectral characteristics of image, characteristics of the sensed objects (dimension, shape and spatial distribution), window size and environmental conditions (Kayitakire et al. 2006; Maltamo et al. 2006; Shamsoddini et al. 2013) and it is difficult to determine the best properties (Shamsoddini et al. 2013). Hence, all GLCM properties for each moving window size were derived.

Model Construction and Validation

The Random Forest algoritm implemented in the “RandomForest” package within demo version of Addinsoft XLStat software was used to model the relationships between the image features exracted remote sensing data and forest structural parameters. The Random Forest method (RF), which was proposed by Breiman (2001), is an ensemble-learning algorithm that combines a large set of regression trees and this algorithm can reduce the overfitting of models. Previous studies have revealed that the RF algorithm has a high prediction accuracy (Zhao et al. 2018; Gao et al. 2019). Therefore, this application has achieved broad popularity lately.

While generating decision trees in the RF algorithm, there are two basic parameters that must be determined by user. These are the number of decision trees (N_{tree}) to be produced and the number of variables (M_{try}) to be tested each time. Since the RO algorithm is computationally efficient, the N_{tree} can be kept as large as possible (Guan et al. 2013). In most of the studies, N_{tree} value is determined as 500 which is default value of algorithm, since errors are fixed until the number of decision trees reaches 500. Also the M_{try} parameter is usually determined to be 1/3 of the number of explanatory variables for regression (Liaw et al. 2002). Explanatory variables are selected automatically in RF algorithm for regression. So that there is no need to select any explanatory variables before modeling.

In the study, after deciding on the best prediction model for forest structural parameters, the prediction error of the final model was estimated by leave-one-out cross-validation method. This method is a suitable validation method when a limited number of data is available for validation (Shamsoddini et al. 2013). In this method, for each forest parameters, one of the sample plots was eliminated from dataset at a time and a model was developed using the n-1 remaining plots. The dependent variables were then estimated for the removed sample

plot. The procedure was repeated for each sample plot. Finally, the coefficient of determination (R^2), and the root mean square error (RMSE) values between observed and predicted forest structural parameters were calculated to assess the overall accuracy of the fitted models.

Results

Using the random forest regression analysis, several prediction models were developed for forest structural variables. All models were statistically significant (*p<0.01*). Table 2 and Figure 3 show the performance of different window sizes for prediction of structural variables in the Black pine stands. In the Black pine stands, it was observed that significant differences between image windows in the estimation accuracy of forest structural variables. Forest structural variables were estimated with R^2 ranging from 0.70 (for window size of 1000 m^2) to 0.86 (for window size of 1000 m^2) using features derived from WorldView-3 satellite image. The 100 m^2 window size performed better for V and BA(R^2 =0.79 and 87 respectively). The 1000 m^2 window size provided the highest accuracy for N (R^2 =0.86). For H, 600 m^2 window size performed relatively better (R^2 =0.75).The prediction accuracy of forest structural variables varied between 0.70 (for 100 m^2 window size) and 0.88 (for 800 m^2 window size) depending on the window size of digital aerial image. The model accuracy generally increased as the window size increased in aerial image. While the 1000 m^2 window size performed better for BA (R^2 =0.86), 600 m2 window size for V (R^2 =0.78) and 800 m^2 window size for N and H (R^2 =0.88 and 0.78) gave better results. The prediction accuracies ranged from 0.76 to 0.84 for LiDAR data depending on the window size. For all structural parameters, the estimation accuracy of the window sizes was almost the same. The R^2 values varied between 0.83 and 0.84 for N, 0.76 and 0.79 for V, 0.80 and 0.81 for BA, and 0.80 and 0.83 for H. Therefore, a significant difference between window sizes could not be determined to estimate the structural parameters for LiDAR dataset.

Table 3 and Figure 4 show the performance of different window sizes for estimation of structural parameters in the Oak stands. The forest structural variables were estimated with R^2 ranging from 0.71 to 0.84 using features derived from WorldView-3 windows. The 100 and 600 m^2 window sizes performed better for V (R^2 =0.80). The 600 m^2 window size provided the highest accuracy for H (R^2 =0.85). Since R^2 values of window sizes were very close to each other in N (0.83 and 0.85) and BA (from 0.71 to 0.75), a significant difference could not be found between window sizes. In the digital aerial image, the 200 m^2 window size for V and BA (R^2 =0.79 and 0.75) and 400 m^2 for H (R^2 =0.85) provided the highest prediction accuracy. On the other hand, no significant difference was found between window sizes for N. However, the prediction accuracy provided by the window sizes of 400 m^2 and 600 m^2 is relatively higher than others. In LiDAR, the R^2 value of window sizes varied between 0.89 and 0.90 for N, 0.86 and 0.87 for V, 0.80 and 0.81 for BA, and 0.89 and 0.90 for H. Therefore, a significant difference could not be determined between window sizes for all structural variables.

Table 4 shows the optimum window sizes for forest structural variables in the selected six window sizes. In our study, the window sizes explained by laser and image metrics of more than 50 percent of the variance was taken into consideration for optimal window size. Among these, the window size with the highest R^2 value was selected as the optimal window size. It appears that the determined optimal window size can be scaled up or down to fit forest canopy components. For example, the optimal window size was determined as 400 m^2 to estimate the V using WorldView-3 in the oak stands. However, 200 m^2 and 600 m^2 window sizes provided the

same or close prediction accuracy. Similarly, optimal window size for estimating N from digital aerial image is 400 m^2. Due to the same or close estimation accuracy, window sizes of 200 m^2 and 600 m^2 can also be selected optimally.

Discussion

This study compared the ability of window sizes to predict the forest structural variables using the remote sensing data. We first built our prediction models using both ground truth dataset and remote sensing datasets. Using these models, N, V, BA and H were estimated for different window sizes in even-aged pure black pine and oak stands. (R^2 values were between 0.70 and 0.88 for black pine and between 0.67 and 0.91 for oak, $p<0.01$). A number of window size ranging from 100 m^2 to 1000 m^2 were tested. Our assumption was that the window size has an effect on the prediction accuracy. This assumption was supported by our findings that the prediction accuracy varies according to different window sizes.

In the WorldView-3 satellite image, significant differences were observed between the prediction accuracies of the image windows for forest structural variables. For each structural variable, all window sizes provided a coefficient of determination greater than 0.70. In the black pine stands, R^2 values calculated for the selected six window sizes showed that the 1000 m^2 window size is more efficient than the other window sizes to estimate the N. The 600 m^2 window size is optimal for H and the 100 m^2 window size is optimal for V and BA. In the case of oak stands, the R^2 values of each moving window size (from 100 m^2 to 1000 m^2) were almost identical for N and BA. This indicates that there was little difference in significance level among the different window sizes. In this case, the appropriate window size can be determined as a size that minimizes a given cost function (Kayitakire et al. 2006) and match stand canopy components (Rich et al. 2010). The R^2 values of 400 and 600 m^2 window sizes were identical for V. Therefore, both can be used as optimal window size to estimate the V. Also, the 600 m^2 window sizes performed better to predict H.

Overall, the performance of large window sizes from digital aerial image was better than small window sizes for estimating forest structural variables. In the black pine stands, the prediction accuracy increases as window size increases, and window sizes larger than 600 m^2 are more efficient than other window sizes for estimation. R^2 values calculated for the selected six window sizes showed that the 800 m^2 window size is optimal for N, the 600 m^2 window size is optimal for V and the 1000 m^2 window size is optimal for BA. The 800 and 1000 m^2 window sizes with same prediction accuracy obtained higher accuracy than smaller window sizes for H. Therefore, one of these two sizes can be used as the optimal window size to estimate H. The window size of 200 m^2 seems optimal for estimating V and BA based on aerial image in the oak stands. While window sizes of 400 and 600 m^2 are optimal for estimating N, 400 m^2 window size is optimal for H.

The prediction accuracy derived from leave-one-out cross-validation for forest structural variables showed that there is generally no significant difference among the different window sizes used for predicting in LİDAR data. Because the R^2 values of each window size were almost identical for all variables in the black pine and oak stands.

There are limited number of published studies on relationships between window size and forest structural variables. These studies used different remote sensing data, different reference data and different analysis

techniques. Hence, it is difficult to compare the results directly. However, studies can be compared to some extent by means of changes in R^2 values, which are considered as indicators of relationship fittings (Castillo-Santiago et al. 2010). The differences with similar studies are probably due to differences in stand structures and tree species composition. Holopainen and Wang (1998) stated that the window size of 20x20 m (400 m^2) is the near-optimal window size for feature extraction from aerial photograph in forest inventory. Kayitakire et al. (2006) reported that the optimum window size for density, height and basal area is 5x5 pixel, 15x15 pixel and 25x25 pixel, respectively. These window sizes provided the highest R^2 values. Steinmann et al. (2013) stated that the window size of 25X25 m (625 m^2) is optimal for estimating the forest growing stock volume using LiDAR data and aerial images. Tonolli et al. (2011) tested different cell sizes (from 20 m to 60 m) to map the tree stem volume using LIDAR data, and it was determined that 40x40 m cell size provided the highest R^2 value as optimal cell size. Meng et al. (2016) used the spectral and texture features extracted from seven different window sizes to estimate the forest structure from the SPOT-5 satellite image. They revealed that the window size of 9x9 pixels is the optimum size for calculating texture statistics. Zhao et al. (2018) concluded that the optimal window size increases as the spatial resolution increases using QuickBird multispectral and panchromatic images.

As a result, the window size which is used to calculate the reference laser and image metrics in prediction of forest structural variables based on remote sensing data, influences the prediction accuracy. The optimal window size varies according to remote sensing data, tree type composition and stand variable to be predicted. The optimal window size can be scaled up or down to fit forest canopy components (Rich et al. 2010).

Conclusion

This study explored the effect of window size on estimation of forest structural variables using airborne LiDAR, digital aerial image and WorldView-3 satellite data. The estimation models were created using ground truth dataset and remote sensing dataset in the black pine and oak stands, and estimation accuracies of stand variables such as stem number, volume, basal area and mean height were calculated for different window sizes. We compared the estimation accuracy for different moving window sizes ranging from 100 m^2 to 1000 m^2 to find the optimal window size. In the digital aerial image and WorldView-3 satellite data, significant differences were observed between the prediction accuracies of the image windows for forest structural variables. However, in the LiDAR data, the prediction accuracy for each moving window size was almost identical. Therefore, there was no significant difference between different sizes. We invite other researchers to do similar studies using different remote sensing data in stands with different structure and species composition.

Abbreviations

BA: Basal Area; **DBH:** Diameter at breast height; **DTM:** Digital Terrain Model; **GLCM**: Grey Level Co-occurence Matrix**; GPS**: Global Positioning System; **H:** Mean Height; **N:** Stem Number; **NDVI**: Normalized Difference Vegetation Index**; NPC**: Normalized Point Cloud; **TIN:** Triangulated Irregular Networks; **R^2**: Coefficient of Determination; **RF:** Random Forest; **V:** Volume

Declarations

Funding

Not applicable.

Availability of data and materials

All data and materials can be obtained by requesting from the author

Authors' contributions

All authors contributed equally to this paper. All authors read and approved the final manuscript.

Ethics approval and consent to participate

Not applicable.

Consent for publication

Not applicable.

Competing interests

The authors declare that they have no competing interests.

References

1. Amini J, Sumantyo JTS (2009) Employing a method on SAR and optical images for forest biomass estimation. IEEE Transactions on Geoscience and Remote Sensing 47:4020-4026.
2. Balenović I, Seletković A, Pernar R, Jazbec A (2015) Estimation of the mean tree height of forest stands by photogrammetric measurement using digital aerial images of high spatial resolution. Annals of Forest Research 58:125-143.
3. Breiman L (2001) Random forests. Machine Learning 45:5-32
4. Castillo-Santiago MA, Ricker M, de Jong BH (2010) Estimation of tropical forest structure from SPOT-5 satellite images. International Journal of Remote Sensing 31:2767-2782.
5. Cho MA, Skidmore AK, Sobhan I, (2009) Mapping beech (Fagus sylvatica L.) forest structure with airborne hyperspectral imagery. Int. J. Appl. Earth Obs. Int. J. Appl. Earth Obs. 11:201-211. doi: 10.1016/j.jag.2009.01.006.
6. Fassnacht FE, Hartig F, Latifi H, Berger C, Hernández J, Corvalán P, Koch B (2014) Importance of sample size, data type and prediction method for remote sensing-based estimations of aboveground forest biomass. Remote Sensing of Environment 154:102-114.
7. García M, Saatchi S, Ustin S, Balzter H (2018) Modelling forest canopy height by integrating airborne LiDAR samples with satellite Radar and multispectral imagery. International Journal of Applied Earth Observation and Geoinformation 66:159-173.

8. Gao X, Wen J, Zhang C (2019) An improved random forest algorithm for predicting employee turnover. Mathematical Problems in Engineering 2019:1-12. doi:10.1155/2019/4140707
9. Guan H, Li J, Chapman M, Deng F, Ji Z, Yang X (2013) Integration of orthoimagery and lidar data for object-based urban thematic mapping using random forests. International Journal of Remote Sensing 34:5166-5186.
10. Harralick RM, Shanmugam K, Dinstein I (1973) Textural features for images classification. IEEE Transactions on Systems, Man and Cybernetics, SMC 6:610-621.
11. Hájek F (2008) Process-based approach to automated classification of forest structures using medium format digital aerial photos and ancillary GIS information. European Journal of Forest Research 127:115-124.
12. Holopainen M, Wang G (1998) The calibration of digitized aerial photographs for forest stratification. International Journal of Remote Sensing 19:677-696.
13. Hyyppa HJ, Hyyppa JM (2001) Effects of stand size on the accuracy of remote sensing-based forest inventory. IEEE Transactions on Geoscience and Remote Sensing 39:2613-2621.
14. Iovan C, Boldo D, Cord M (2008) Detection, characterization, and modeling vegetation in urban areas from high-resolution aerial imagery. IEEE Journal of Selected Topics in Applied Earth Observations and Remote Sensing 1:206-213.
15. Joshi NP, Mitchard ET, Schumacher J, Johannsen VK, Saatchi S, Fensholt R (2015) L-band SAR backscatter related to forest cover, height and aboveground biomass at multiple spatial scales across Denmark. Remote Sensing 7:4442-4472.
16. Junttila V, Finley AO, Bradford JB, Kauranne T (2013) Strategies for minimizing sample size for use in airborne LiDAR-based forest inventory. Forest Ecology and Management 292:75-85.
17. Kayitakire F, Hamel C, Defourny P (2006) Retrieving forest structure variables based on image texture analysis and IKONOS-2 imagery. Remote Sensing of Environment 102:390-401.
18. Koch B, Straub C, Dees M, Wang Y, Weinacker H (2009) Airborne laser data for stand delineation and information extraction. International Journal of Remote Sensing 30:935-963.
19. Kwak DA, Lee WK, Lee JH, Biging GS, Gong P (2007) Detection of individual trees and estimation of tree height using LiDAR data. Journal of Forest Research 12:425-434.
20. Liaw A, Wiener M (2002) Classification and regression by randomForest. R News, 2:18-22.
21. Lee H, Slatton KC, Roth BE, Cropper Jr WP (2010) Adaptive clustering of airborne LiDAR data to segment individual tree crowns in managed pine forests. International Journal of Remote Sensing 31:117-139.
22. Lidar360 (2018) Lidar360 User Guide. GreenValley Int., California.
23. Maltamo M, Malinen J, Packalén P, Suvanto A, Kangas J (2006) Nonparametric estimation of stem volume using airborne laser scanning, aerial photography, and stand-register data. Canadian Journal of Forest Research 36:426-436.
24. Meng J, Li S, Wang W, Liu Q, Xie S, Ma W (2016) Estimation of forest structural diversity using the spectral and textural information derived from SPOT-5 satellite images. Remote Sensing 8(125):1-24.
25. Morgan JL, Gergel SE (2010) Quantifying historic landscape heterogeneity from aerial photographs using object-based analysis. Landscape Ecology 25:985-998.

26. Næsset E (2002) Predicting forest stand characteristics with airborne scanning laser using a practical two-stage procedure and field data. Remote Sensing of Environment 80:88-99.
27. Ozdemir I, Donoghue DNM (2013) Modelling Tree Size Diversity from Airborne Laser Scanning using Canopy Height Models with Image Texture Measures. Forest Ecology and Management 295:28-37.
28. Ozdemir I, Karnieli A (2011) Predicting forest structural parameters using the image texture derived from WorldView-2 multispectral imagery in a dryland forest, Israel. International Journal of Applied Earth Observation and Geoinformation 13:701-710.
29. Ozkan UY, Ozdemir I, Saglam S, Yesil A, Demirel T (2016) Evaluating the woody species diversity by means of remotely sensed spectral and texture measures in the urban forests. Journal of the Indian Society of Remote Sensing 44:687-697.
30. Ozkan UY, Demirel T (2018) Estimation of forest stand parameters by using the spectral and textural features derived from digital aerial images. Applied Ecology and Environmental Research 16:3043-3060.
31. Ozkan UY, Demirel T, Ozdemir I, Saglam S, Mert A (2020) Examining LiDAR–WorldView-3 data synergy to generate a detailed stand map in a mixed forest in the north-west of Turkey. Advances in Space Research 65:2608-2621.
32. Pascual C, García-Abril A, García-Montero LG, Martín-Fernández S, Cohen WB (2008) Object-based semi-automatic approach for forest structure characterization using lidar data in heterogeneous Pinus sylvestris stands. Forest Ecology and Management 255:3677-3685.
33. PCI Geomatics (2017) Geomatica Help. PCI Geomatics, Ontario.
34. Rich RL, Frelich L, Reich PB, Bauer ME (2010) Detecting wind disturbance severity and canopy heterogeneity in boreal forest by coupling high-spatial resolution satellite imagery and field data. Remote Sensing of Environment 114:299-308.
35. Ruiz LA, Hermosilla T, Mauro F, Godino M (2014) Analysis of the influence of plot size and LiDAR density on forest structure attribute estimates. Forests 5:936-951.
36. Robinson C, Saatchi S, Neumann M, Gillespie T (2013) Impacts of spatial variability on aboveground biomass estimation from L-band radar in a temperate forest. Remote Sensing 5:1001-1023.
37. Saarela, S, Wästlund, A, Holmström, E, Mensah, A. A, Holm, S, Nilsson, M, Fridman, J, Ståhl G (2020) Mapping aboveground biomass and its prediction uncertainty using LiDAR and field data, accounting for tree-level allometric and LiDAR model errors. Forest Ecosystems 7(1): 1-17.
38. Shamsoddini A, Trinder JC, Turner R (2013) Pine plantation structure mapping using WorldView-2 multispectral image. International Journal of Remote Sensing 34:3986-4007.
39. Steinmann K, Mandallaz D, Ginzler C, Lanz A (2013) Small area estimations of proportion of forest and timber volume combining Lidar data and stereo aerial images with terrestrial data. Scandinavian Journal of Forest Research 28:373-385.
40. Su, H, Shen, W, Wang, J, Ali, A, Li M (2020) Machine learning and geostatistical approaches for estimating aboveground biomass in Chinese subtropical forests. Forest Ecosystems, 7(1): 1-20.
41. Tonolli S, Dalponte M, Vescovo L, Rodeghiero M, Bruzzone L, Gianelle D (2011) Mapping and modeling forest tree volume using forest inventory and airborne laser scanning. European Journal of Forest Research 130:569-577.

42. Zald HS, Ohmann JL, Roberts HM, Gregory MJ, Henderson EB, McGaughey RJ, Braaten J (2014) Influence of lidar, Landsat imagery, disturbance history, plot location accuracy, and plot size on accuracy of imputation maps of forest composition and structure. Remote Sensing of Environment 143:26-38.
43. Zenner EK, Peck JE (2009) Characterizing structural conditions in mature managed red pine: spatial dependency of metrics and adequacy of plot size. Forest Ecology and Management 257:311-320.
44. Zhao Q, Wang F, Zhao J, Zhou J, Yu S, Zhao Z (2018) Estimating Forest Canopy Cover in Black Locust (Robinia pseudoacacia L.) Plantations on the Loess Plateau Using Random Forest. Forests 9(623):1-16.

Tables

Table 1 The descriptive statistics of the forest structural variables in sample plots

Stand	Variables	Minimum	Maximum	Mean	SD
Black Pine	N (ha^{-1})	525	1350	959	240
	BA (m^2 ha^{-1})	27,36	49,28	37,91	6,33
	V (m^3 ha^{-1})	144,60	451,66	226,63	68,38
	H (m)	9,50	20,30	11,97	2,32
Oak	N (ha^{-1})	550	1700	1115	286
	BA (m^2 ha^{-1})	18,74	37,35	24,86	3,73
	V (m^3 ha^{-1})	150,25	366,58	223,16	50,60
	H (m)	13,00	18,00	15,33	1,32

Table 2 Prediction results of the forest structural variables according to different window sizes (Black pine stands)

Forest variables	Window size	WorldView-3			Aerial image			LiDAR		
		R^2	RMSE	RMSE%	R^2	RMSE	RMSE%	R^2	RMSE	RMSE%
N	100	0.78	109.37	11.40	0.80	103.59	10.80	0.84	94.75	9.87
	200	0.73	120.92	12.60	0.80	105.55	11.00	0.84	93.23	9.72
	400	0.79	108.45	11.30	0.84	93.90	9.79	0.83	96.97	10.11
	600	0.80	103.79	10.82	0.86	87.72	9.14	0.83	95.60	9.96
	800	0.82	100.33	10.46	0.88	82.68	8.62	0.84	94.79	9.88
	1000	0.86	87.24	9.09	0.83	95.31	9.93	0.84	94.57	9.86
V	100	0.79	30.50	13.46	0.77	31.30	13.81	0.76	32.62	14.39
	200	0.75	33.27	14.68	0.75	33.28	14.69	0.78	31.21	13.77
	400	0.74	33.84	14.93	0.74	33.97	14.99	0.79	30.51	13.46
	600	0.77	32.24	14.23	0.78	31.36	13.84	0.79	30.83	13.60
	800	0.77	31.78	14.02	0.75	33.53	14.80	0.79	31.10	13.72
	1000	0.78	31.63	13.95	0.76	32.53	14.36	0.77	31.72	13.99
BA	100	0.87	2.19	5.78	0.82	2.64	6.97	0.80	2.78	7.33
	200	0.82	2.62	6.92	0.76	3.01	7.94	0.81	2.68	7.08
	400	0.81	2.71	7.15	0.79	2.85	7.53	0.80	2.74	7.23
	600	0.79	2.80	7.38	0.81	2.67	7.05	0.81	2.64	6.97
	800	0.76	3.04	8.03	0.82	2.63	6.94	0.81	2.73	7.19
	1000	0.78	2.88	7.59	0.86	2.31	6.11	0.81	2.71	7.15
H	100	0.74	1.16	9.66	0.70	1.24	10.33	0.83	0.94	7.82
	200	0.73	1.17	9.76	0.74	1.16	9.68	0.83	0.94	7.83
	400	0.71	1.23	10.27	0.76	1.12	9.36	0.82	0.97	8.14
	600	0.75	1.14	9.53	0.76	1.10	9.19	0.80	1.02	8.55
	800	0.74	1.16	9.70	0.78	1.06	8.84	0.80	1.01	8.48
	1000	0.70	1.23	10.31	0.78	1.05	8.80	0.81	0.99	8.24

Table 3 Prediction results of the forest structural variables according to different window sizes (Oak stands)

Forest variables	Window size	Aerial image			LiDAR					
		R^2	RMSE	RMSE%	R^2	RMSE	RMSE%	R^2	RMSE	RMSE%
N	100	0.84	110.55	9.92	0.90	87.67	7.87	0.89	91.34	8.20
	200	0.84	112.58	10.10	0.90	89.56	8.04	0.90	87.54	7.85
	400	0.83	114.38	10.26	0.92	79.37	7.12	0.89	90.91	8.16
	600	0.84	110.47	9.91	0.92	81.14	7.28	0.90	90.13	8.09
	800	0.84	111.87	10.04	0.91	83.60	7.50	0.89	92.92	8.34
	1000	0.84	110.93	9.95	0.91	83.29	7.47	0.90	86.34	7.75
V	100	0.77	23.79	10.66	0.72	26.27	11.77	0.87	17.61	7.89
	200	0.78	23.00	10.31	0.79	22.61	10.13	0.87	17.98	8.06
	400	0.80	22.23	9.96	0.76	24.07	10.78	0.86	18.64	8.35
	600	0.80	22.21	9.95	0.74	25.16	11.27	0.87	17.94	8.04
	800	0.76	24.10	10.80	0.73	25.89	11.60	0.86	18.64	8.35
	1000	0.78	23.32	10.45	0.71	26.61	11.92	0.86	18.59	8.33
BA	100	0.73	1.91	7.68	0.68	2.08	8.35	0.81	1.59	6.39
	200	0.75	1.84	7.42	0.75	1.81	7.29	0.81	1.59	6.41
	400	0.74	1.87	7.52	0.70	2.00	8.06	0.80	1.62	6.51
	600	0.75	1.83	7.34	0.68	2.07	8.31	0.81	1.60	6.44
	800	0.71	1.97	7.93	0.68	2.08	8.36	0.80	1.62	6.50
	1000	0.75	1.83	7.35	0.67	2.09	8.41	0.80	1.62	6.53
H	100	0.77	0.62	4.04	0.80	0.58	3.77	0.89	0.43	2.82
	200	0.83	0.53	3.46	0.79	0.59	3.87	0.90	0.41	2.66
	400	0.82	0.54	3.55	0.85	0.50	3.24	0.88	0.44	2.89
	600	0.85	0.49	3.21	0.81	0.56	3.64	0.89	0.42	2.73
	800	0.82	0.54	3.52	0.79	0.59	3.82	0.89	0.43	2.77
	1000	0.81	0.56	3.66	0.77	0.62	4.07	0.90	0.42	2.72

Table 4 The optimum window sizes for forest structural variables

	Forest variables	Optimal Window Sizes (m^2)		
		WorldView-3	Aerial image	LiDAR
Black pine	N	1000	800	100-1000
	V	100	600	400-800
	BA	100	1000	100-1000
	H	600	800-1000	100-200
Oak	N	100-1000	400-600	100-1000
	V	400-600	200	100-1000
	BA	100-1000	200	100-1000
	H	600	400	100-1000

Figures

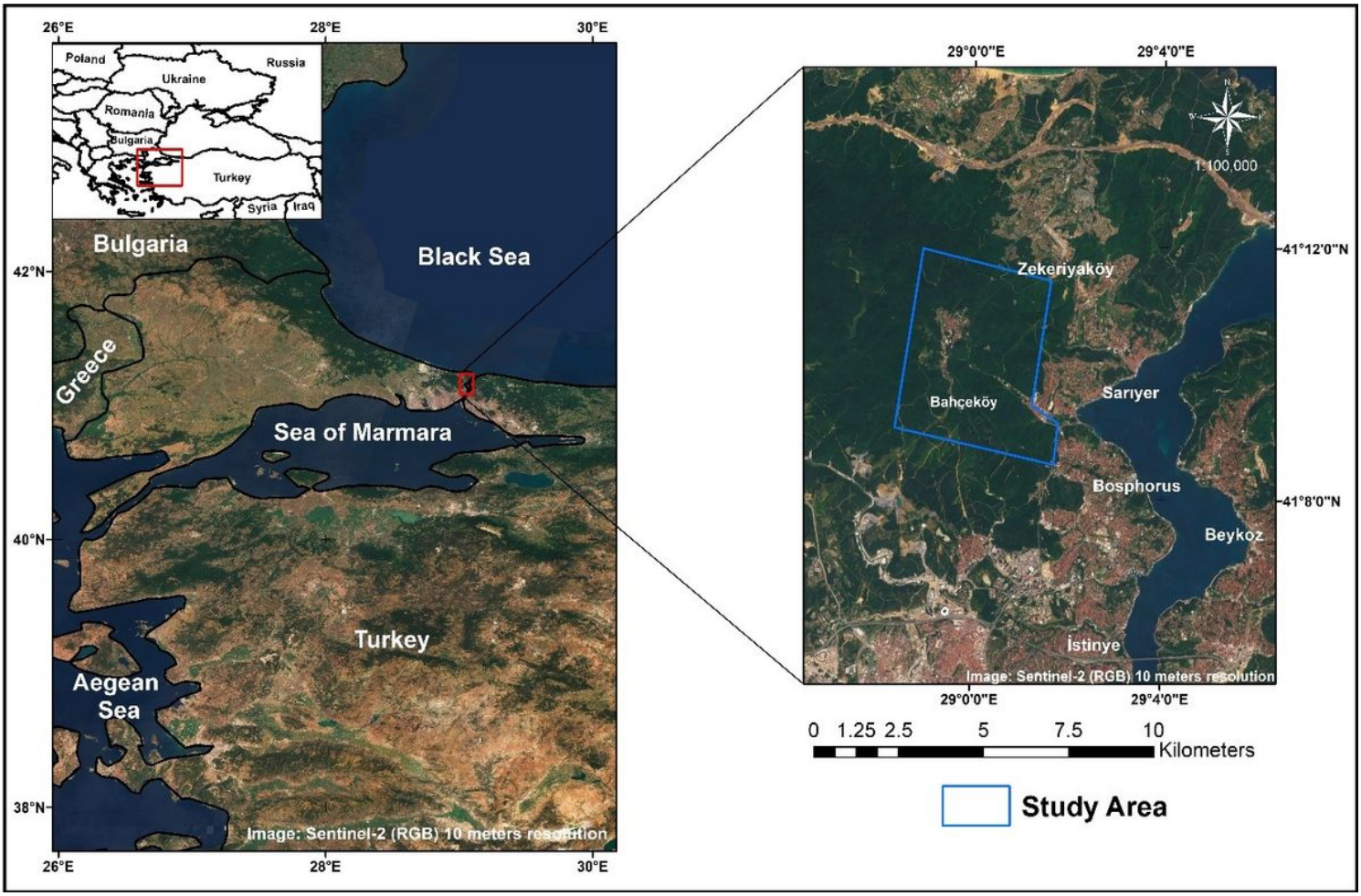

Figure 1

Study area Note: The designations employed and the presentation of the material on this map do not imply the expression of any opinion whatsoever on the part of Research Square concerning the legal status of any country, territory, city or area or of its authorities, or concerning the delimitation of its frontiers or boundaries. This map has been provided by the authors.

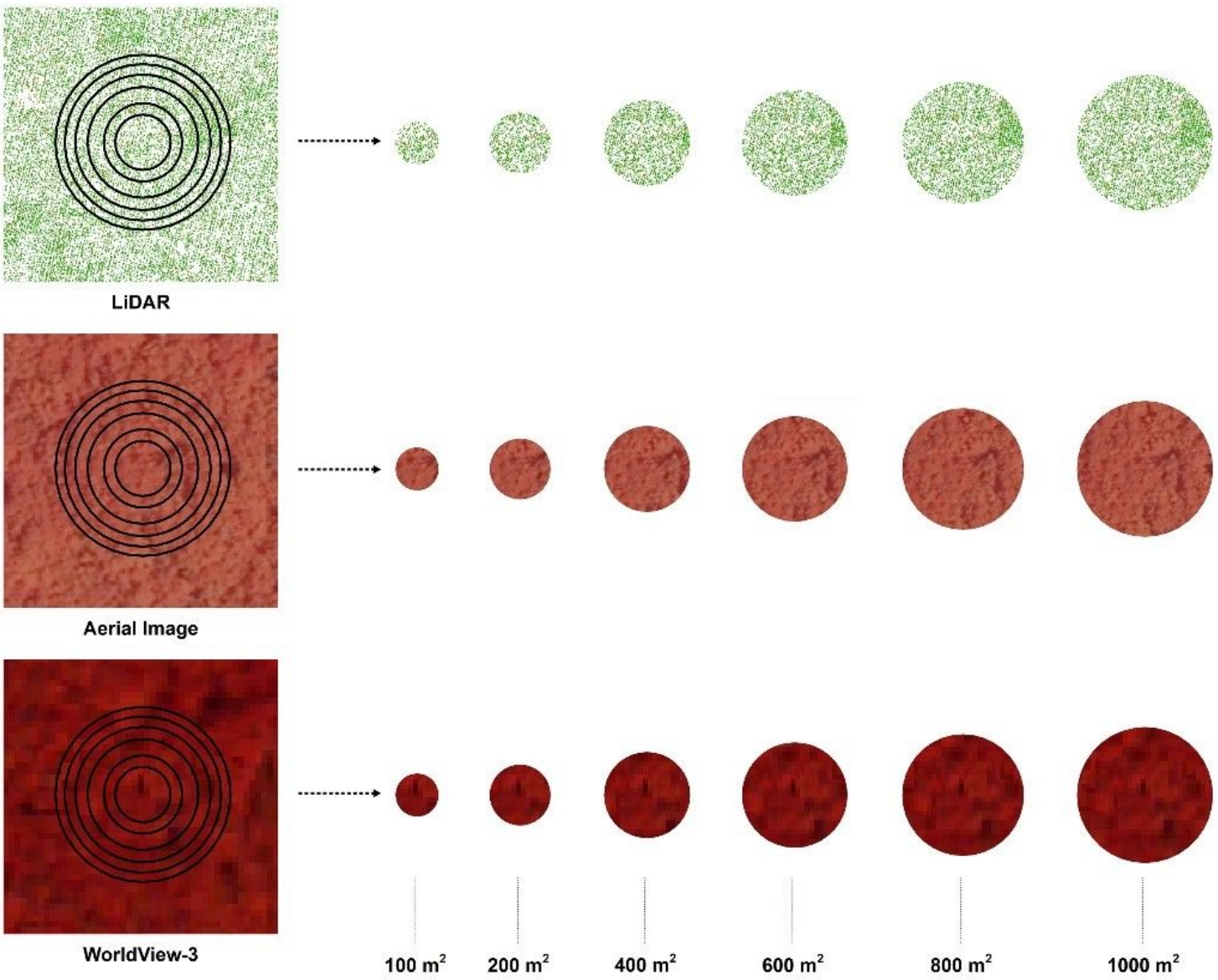

Figure 2

Application of window sizes of remote sensing data

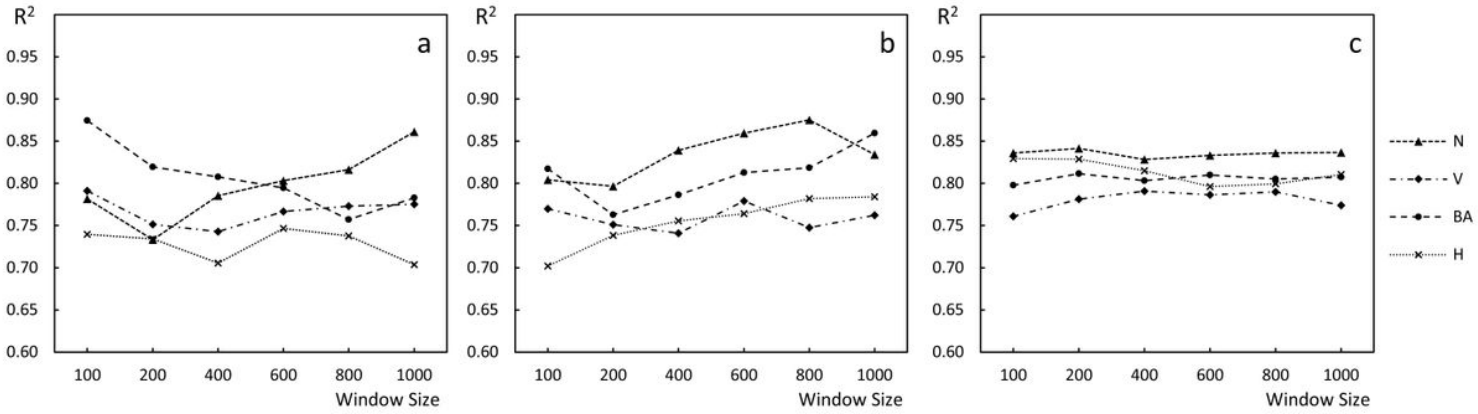

Figure 3

Illusration of the window size effect on the prediction of the forest structural variables a) WorldView-3 b) Aerial image c) LiDAR (Black pine stands)

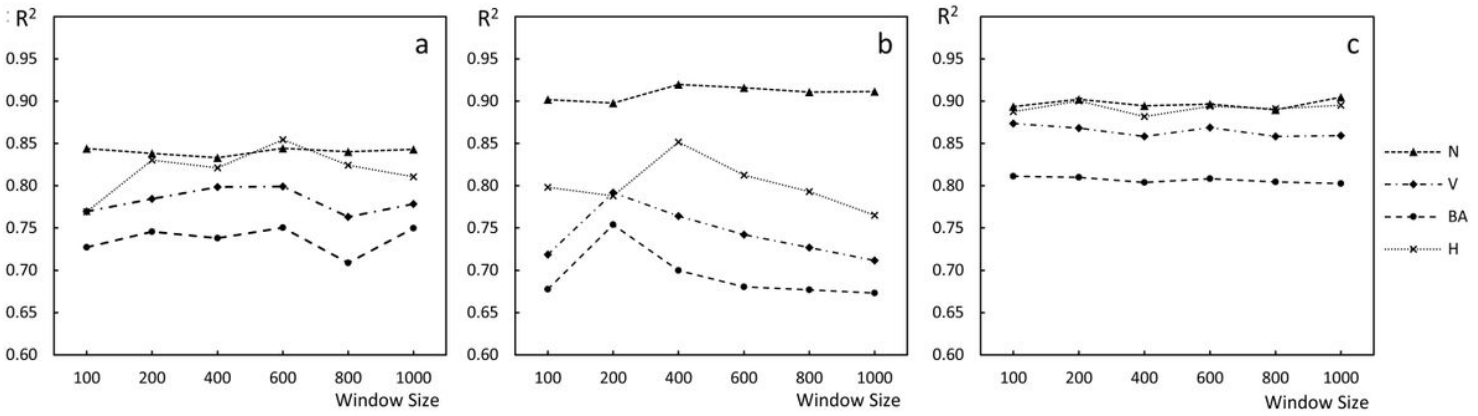

Figure 4

Illusration of the window size effect on the prediction of the forest structural variables a) WorldView-3 b) Aerial image c) LiDAR (Oak stands)